Study of Temperature-Dependent Angular Goos-Hanchen Effect on the Surface of Graphene-Vanadium Dioxide

By

Momina Nisar

Department of Electronics,

Quaid-i-Azam University, Islamabad, 45320, Pakistan

This dissertation is submitted for the degree of
Master of Philosophy

September 2023

Certificate

It is certified that the work presented in this dissertation is accomplished by Momina Nisar under the supervision of Prof. Qaisar Abbas Naqvi at Quaid-i-Azam University, Islamabad, Pakistan.

Supervisor:

_____

Prof. Qaisar Abbas Naqvi
Professor
Department of Electronics,
Quaid-i-Azam University, Islamabad, Pakistan.

Submitted through:

_____

Prof. Qaisar Abbas Naqvi
Chairman
Department of Electronics,
Quaid-i-Azam University, Islamabad, Pakistan.

Acknowledgment

Abstract

The objective of the work is to investigate the behavior of the angular Goos–Hanchen (GH) effect for a planar graphene-vanadium dioxide geometry, taking into account the temperature and wavelength dependency. A monochromatic Gaussian beam of light is used as a source of excitation. Experimental results from a published work have been used to incorporate the temperature dependency of vanadium dioxide. In addition, wavelength-dependent experimental results of permittivity at a particular value of temperature for vanadium dioxide are used. Mathematical expressions for the angular GH effect are derived. The behavior of angular and modified angular GH effects and their difference are studied in detail. The modified GH effect is obtained by passing reflected waves through a polarizer. It is established that vanadium dioxide has special characteristics depending on temperature; it behaves as a metal at high temperatures and dielectric at low temperatures. Additionally, it possesses a hysteresis state describing a metal-dielectric transformation by heating or cooling the substrate, which provides an excellent opportunity to adjust and control the angular GH effect according to application requirements.

Contents

List of Figures

Chapter 1

Introduction

The Goos-Hänchen shift (GHS) is a spatial/angular displacement covered by a beam of light across the interface between two different media. The GHS occurs when a beam of light incident from an optically denser to a rarer medium which leads the light to briefly penetrate into the second medium and then laterally displaces at reflection. This lateral displacement may be forward (positive GHS) or backward (negative GHS) mainly depending upon the characteristics of the considered interface. Issac Newton speculated about the lateral shift in his book "Newton Optics" [1] and later on in 1947, Goos and Hänchen [2] experimented to prove Newton's conjecture. They found lateral shift was most prominent near critical and brewster angles where total internal reflection and minimum reflection occur respectively.

   After a year of this genius experiment, Artman [3] presented a theoretical formula known as the stationary-phase method to evaluate GHS which is based on a mathematical argument about the frequency and wavenumber spectrum. Renard [4] established a theoretical approach called the conventional energy-flux method to confirm the consistency of the predictions by the stationary-phase method. The conventional energy-flux method reported a major flaw which was later updated by Yasumoto and Oishi [5] from the point of view of the conservation of energy. A beam reflected off an interface experiences spatial and angular shifts depending on the polarization and the beam profile. Spatial displacement is the well-known GHS in the plane of incidence exclusively depending on the polarization while angular shifts that depend on the beam profile were recently demonstrated by Merano et al. [6]. Although the GHS has been known for a long time, it has recently come to the scientific community's attention due to its major contribution to the advance-

ment of technology and has been widely investigated in non-linear optics [7], plasma physics [8], surface physics [9], and quantum mechanics [10]. The breakthrough in manipulating GHS dispensed a variety of applications like bar code encryption [11], optical switches [12], and optical heterodyne sensors [13]. In addition, there has been growing interest in the medical field such as cancer detection by GHS-based sensors which is addressed in [14]. The design process of GHS-based optical devices demands strong control and adjustment of this optical phenomenon and also in some applications GHS needs to be significantly enhanced. To obtain the aforementioned characteristics, researchers have been investigating GHS across different optical structures including left-handed materials [15], topological insulators [16], epsilon-near-zero metamaterials [17], [18], [19], magneto-optical materials [20], general medium [21], and dispersive media [22].

Graphene is a recently discovered two-dimensional material made up of a single layer of carbon atoms forming a hexagonal pattern [23] with distinct electrical, mechanical, and chemical properties [24]. Having remarkable electronic characteristics, graphene's optical response can be precisely controlled by external forces like chemical doping or electrical gating [25]. The energy band structure of the electrons in carbon atoms determines graphene's conductivity [26].

Pure graphene can be regarded as a metal with an empty valance band and as a zero-gap semiconductor because of its energy band structures. This duality picture makes graphene particularly interesting for applications in many photonic devices that require conducting but transparent thin films. With great potential, graphane has been widely explored in the last few years even though it was only isolated for the first time in 2004 [24]. Following the discovery, several theoretical studies are reported such as Neto et al.'s review of electronic properties [27], and more focused on electronic transport properties [28]. To explore graphene's characteristics more deeply, experimental activities are performed including Raman characterization methods [29], a detailed discussion of synthesis [30], and transport mechanisms [31], [32]. The exploration of graphene at an extensive level led to applications of optoelectronic technologies [33], transistors, and related bandgap engineering [34]. Logic transistor technology has greatly revolutionized by incorporating graphene in the channel region of transistors which due to its monoatomic thickness reduces parasitic effects including punch-through effects, velocity saturation effects, and hot electron effects [34]. Modern graphene-based field-effect transistors have short channel lengths that result in high elec-

trical fields of around $\approx$100kV/cm which excite the optical phonon mode of graphene to enhance device performance [31]. In addition to transistor technologies, considerable research has also been done on graphene sensors. The graphene-based nanomaterials exhibit extraordinary sensitivity to adsorbed materials [35] which has benefited to developed electrochemical sensors [36] and biosensors [37]. Graphene has shown improved optical response and GHS with its less complexity has resulted in scrutiny of this optical phenomenon across numerous graphene-based structures [19], [38], [39], [40].

In the field of material sciences and liquid-state physics, vanadium dioxide (VO_2) is an interesting substance that has garnered a lot of attention because of its exceptional and remarkable properties. It is a chemical combination of the elements vanadium and oxygen. VO_2 is a material of interest among a number of researchers because of its ability to switch between monoclinic (dielectric) and tetragonal (metal) substances by cooling the substrate at $T < 58^oC$ [41] and heating at $T > 72^oC$ [42] respectively. When the temperature values between 58^oC and 72^oC, the purely monoclinic to purely tetragonal transition happens which is a reversible but hysteretic process, though its reliance on the warming rate has not been yet completely perceived [43]. Generally, the thermal-hysteresis regime $58^oC{\leq}T{\leq}72^oC$ is avoided during the study on devices containing VO_2. Electromagnetically, VO_2 is a function of wavelength such as it transforms from a dissipative dielectric to another dissipative dielectric if the free-space wavelength is $\lambda_0 < 1100$ nm while it transforms from a dissipative dielectric to a plasmonic metal (or vice versa) if $\lambda_0 > 1100$ nm [44]. In addition, the important feature of VO_2 is that the complex permittivities of its two crystallographic phases close to the infrared range are remarkably different [45] which change with the decrease of wavelength from 800 nm to 1550 nm at the particular range of temperature. These properties make it a promising material for a wide range of practical applications. The oxides of vanadium such as VO_2, V_2O_3 and V_2O_5 are low cost with unique lamellar or layered structures have been used in supercapacitors and batteries [46]. VO_2 contains multivalent stable oxidation resulting in the formation of several compositions with tremendous properties such as optical, magnetic, and structural transformation [47]. With high specific capacities/energies, VO_2 has been utilized in energy storage devices [48]. Moreover, VO_2 possesses rapid metal-insulator transition characteristics at specific temperature values which change its electronic properties yielding intelligent window coatings, memristors, and switching applications [49]. It is possible to create terahertz devices with adjustable characteristics using

VO_2-graphene hybrids. VO_2 could be used in some interesting ways when paired with graphene to control and adjust GHS which may be applicable for photonic switching and modulation.

To report this research, we explore the angular GHS for a planar interface involving graphene and VO_2 substrate by taking into consideration the influence of temperature and wavelength. A monochromatic Gaussian light beam is used as a source of excitation. Existing experimental data from literature has been utilized to incorporate the temperature sensitivity of VO_2. Furthermore, experimental permittivity values specific to a particular temperature of VO_2 are incorporated, considering their dependence on wavelength. Mathematical expressions for angular GHS, modified angular GHS, and their difference are derived and thoroughly analyzed for different parameters related to the considered framework. The modified GHS is achieved by directing reflected waves through a polarizer. It's noteworthy that vanadium dioxide exhibits a hysteresis state, indicating a metal-dielectric transition due to heating or cooling. This property offers a valuable opportunity to tailor and regulate the angular GHS as per specific application needs.

1.1 Proposed Work

In graphene, we are going to observe the angular GH shifts and their relation with incident angle. Furthermore, the connection between the magnitude of the Brewster angle and external conditions of the magnetic field will be discussed. As vanadium dioxide is a temperature-dependent substrate, we will check the behavior of angular GHS and modified angular GHS and the difference between them at different temperatures and wavelengths.

4

Chapter 2

Model and Formulation

Figure 1 illustrates a schematic diagram of wave reflection at graphene-based VO_2 planar substrate placed in air. The monochromatic Gaussian light beam impinges with an incident angle θ_i from air to the interface (y=0), which separates air in the region (y>0) from VO_2 planar substrate covered with a graphene sheet. The applied beam contains a static magnetic field along the y direction that is normal to the interface. The incident and reflected beam's electromagnetic field components are denoted by (x_i, y_i, z_i) and (x_r, y_r, z_r)
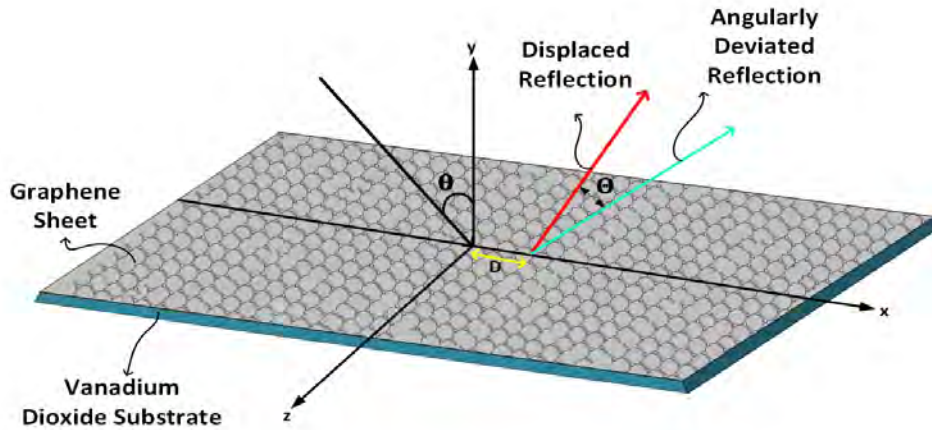

Figure 2.1: The Schematic Diagram of Wave Reflection at Graphene-Vanadium Dioxide Interface.

respectively. The amplitude of the electric field associated with the beam can be written as follows [50],

$$\widetilde{E_i} \propto \exp\left[iky_i - \frac{k}{2}\frac{x_i^2 + z_i^2}{Z_R + iy_i}\right] \times (\hat{x}_i f_p + \hat{z}_i f_s). \tag{2.1}$$

where $Z_R = \pi w_o^2/\lambda$ is the Rayleigh range while k, λ and w_o represent wavenumber, incident wavelength, and beam width, respectively. The polarization of the beam is determined by the unit vector $\hat{f} = (\hat{x}_i f_p + \hat{z}_i f_s)/\sqrt{|f_p|^2 + |f_s|^2}$ where $f_s = a_s$ and $f_p = a_p$ representing amplitudes of perpendicular and parallel polarization, respectively.

The reflection coefficients can be expanded as a polynomial of k_{ix} using the Taylor series expansion based on the arbitrary angular spectrum component. The Fourier transformations can then be used to solve the reflected field and can be expressed as,

$$\begin{aligned}
\mathbf{E_r} \propto \exp&\left(iky_r - \frac{k}{2}\frac{x_r^2 + z_r^2}{Z_R + iy_r}\right) \\
&\times \left\{\left[f_p r_{pp}\left(1 - \frac{ix_r}{Z_R + iy_r} \times \frac{\partial lnr_{pp}}{\partial\theta_i}\right)\right.\right. \\
&\left.+ f_s r_{ps}\left(1 - \frac{ix_r}{Z_R + iy_r} \times \frac{\partial lnr_{ps}}{\partial\theta_i}\right)\right]\hat{x}_r \\
&+ \left[f_s r_{ss}\left(1 - \frac{ix_r}{Z_R + iy_r} \times \frac{\partial lnr_{ss}}{\partial\theta_i}\right)\right. \\
&\left.\left.+ f_p r_{sp}\left(1 - \frac{ix_r}{Z_R + iy_r} \times \frac{\partial lnr_{ps}}{\partial\theta_i}\right)\right]\hat{z}_r\right\}.
\end{aligned} \tag{2.2}$$

where r_{sp} and r_{ps} denote cross-polarization reflection coefficients while r_{ss} and r_{pp} represent reflection coefficients for perpendicular and parallel polarization, respectively.

The reflected electric field angular spectrum is connected to the boundary distribution [51] as,

$$\begin{bmatrix} \widetilde{E_r^p} \\ \widetilde{E_r^s} \end{bmatrix} = \begin{bmatrix} r_{pp} & r_{ps} \\ r_{sp} & r_{ss} \end{bmatrix} \cdot \begin{bmatrix} \widetilde{E_i^p} \\ \widetilde{E_i^s} \end{bmatrix} \tag{2.3}$$

The Fresnel reflection coefficients of graphene-based VO_2 system are obtained by applying boundary conditions as,

$$r_{pp} = \frac{(k_{ty} + k_{iy} + \omega\mu_a\sigma_T)(k_{iy}\epsilon_b - k_{ty}\epsilon_a) + \mu_a k_{iy}k_{ty}\sigma_H^2}{(k_{ty} + k_{iy} + \omega\mu_a\sigma_T)(k_{iy}\epsilon_b + k_{ty}\epsilon_a) + \mu_a k_{iy}k_{ty}\sigma_H^2},$$

$$r_{ss} = -\frac{(k_{ty} - k_{iy} + \omega\mu_a\sigma_T)(k_{iy}\epsilon_b + k_{ty}\epsilon_a) + \mu_a k_{iy}k_{ty}\sigma_H^2}{(k_{ty} + k_{iy} + \omega\mu_a\sigma_T)(k_{iy}\epsilon_b + k_{ty}\epsilon_a) + \mu_a k_{iy}k_{ty}\sigma_H^2},$$

$$r_{ps} = r_{sp} = -2\sqrt{\frac{\mu_a}{\epsilon_a}} \times$$

$$\frac{k_{iy}k_{ty}\sigma_H}{(k_{ty} + k_{iy} + \omega\mu_a\sigma_T)(k_{iy}\epsilon_b + k_{ty}\epsilon_a) + \mu_a k_{iy}k_{ty}\sigma_H^2}. \tag{2.4}$$

where $k_{iy} = k_i \cos\theta_i$ and $k_{ty} = k_t \cos\theta_t$, while θ_t is the refraction angle. The permeability of both media is μ_a meanwhile ϵ_a/ϵ_b denotes the permittivity of air/graphene-based VO_2 system. Moreover, σ_T/σ_H is the transverse/Hall conductivity while Hall conductivity of graphene can be represented in the form of the external magnetic field as,

$$\sigma_H = (4n_c + 2)sgn[B]\frac{e^2}{2\pi\hbar}. \tag{2.5}$$

here, $\hbar$ in the above equation is Planck's constant while n_c is used to represent the quantized energy levels for electrons in magnetic fields and plays an important role in σ_H of graphene.

$$n_c = Int\left[\frac{\mu_f^2}{ev_f^2|B|2\hbar}\right]. \tag{2.6}$$

whereas v_f and μ_f is the Fermi velocity and energy, respectively. The longitudinal displacement of the field centroid at a given plane can be written as [52],

$$d_{GH} = \frac{\int\int(x_r I(x_r, y_r, z_r)dx_r dz_r)}{\int\int(I(x_r, y_r, z_r)dx_r dz_r)}. \tag{2.7}$$

The flux of the time-averaged Poynting vector $\mathbf{S}$ is closely linked to the beam intensity spatial profile as follows,

$$I(x_r, y_r, z_r) \propto \mathbf{S}.\hat{y}_r \tag{2.8}$$

The expressions of GHS for both polarizations can be obtained from Eq. (7), the details given in [52] are omitted in order to simplify the calculations as,

$$d_{GH} = \frac{2(R_{pp/ss}^2 \varphi_{pp/ss} + R_{ps/sp}^2 \varphi_{ps/sp}) Z_R}{2k(R_{ps/sp}^2 + R_{pp/ss}^2) Z_R + \chi_{pp/ss} + \chi_{ps/sp}}$$

$$-y_r \frac{2(R_{pp/ss}^2 \rho_{pp/ss} + R_{ps/sp}^2 \rho_{ps/sp})}{2k(R_{ps/sp}^2 + R_{pp/ss}^2) Z_R + \chi_{pp/ss} + \chi_{ps/sp}}. \tag{2.9}$$

whereas, $r_m = R_m \exp(i\phi_m)$, $R_m = |r_m|$, $\phi_m = arg(r_m)$, $\chi_m = R_m^2 (\varphi_m^2 + \rho_m^2)$, $\rho_m = Re(\frac{\partial lnr_m}{\partial \theta_i})$, $\varphi_m = Im(\frac{\partial lnr_m}{\partial \theta_i})$, $m \in \{ss, pp, sp, ps\}$. The first term in Eq. (9), is the spatial GHS while the second term gives the important expression for angular GHS as,

$$\Theta_{GH} = -\frac{2(R_{pp/ss}^2 \rho_{pp/ss} + R_{ps/sp}^2 \rho_{ps/sp})}{2k(R_{ps/sp}^2 + R_{pp/ss}^2) Z_R + \chi_{pp/ss} + \chi_{ps/sp}}. \tag{2.10}$$

The modified angular GHS can be obtained by eliminating cross-polarization components in the above expression as,

$$\Theta_{GH}' = -\frac{2(R_{pp/ss}^2 \rho_{pp/ss})}{2k(R_{pp/ss}^2) Z_R + \chi_{pp/ss}}. \tag{2.11}$$

Chapter 3

Results And Discussion

In this section, the main focus is to numerically analyze how incident angle/wavelength/beamwidth, temperature, external magnetic field, and Fermi energy work as effective tuning agents to modulate angular/modified angular GHSs (collectively called angular shifts). The analysis encompasses three different scenarios where VO_2 beneath the graphene sheet behaves differently, as shown in Table 1.

It is more important to briefly study the behavior of reflectance before examining angular shifts. The numerical results are only analyzed for horizontal polarization to make the discussion more manageable. Figure 2 displays the impact of incident wavelength on reflectance as a function of incident angle and external magnetic field for Case 1, as mentioned in Table 1. From the figure, it appears that the reflectance behavior is most sensitive between 85 and 95 degrees of the incident angle when the incident wavelength is changed. Moreover, a pseudo-Brewster angle is also being observed in this range. Additionally, the change in amplitude of reflectance of the electromagnetic wave is responsible for angular GHS since in the above range (i.e., between 85 and 95), remarkable angular shifts would be generated.

Figure 3 corresponds to Case 1 and depicts the impact of incident wavelength on angular shifts. The above-mentioned incident angle regime is quite important, where the positive and negative angular shifts are noticed that tend to increase as the incident wavelength increases. Moreover, a negative peak is observed in the behavior of modified angular GHS near the pseudo-Brewster angle. In addition, modified angular GHS enhanced along with a narrow-width negative peak when the incident wavelength increases. This phenomenon represents angular shifts are strongly sensitive to incident

Case	Temperature (T)	Behaviour	Incidence Wave-length (λ)	Permittivity (ϵ_b)
1.	T > 72°C	Metal	800nm	-32.8+0.46ι
			1550nm	-140.4+3.56ι
2.	T < 58°C	Dielectric	800nm	32.8+0.46ι
			1550nm	140.4+3.56ι
3. (i)	50°C≤T≤80°C	Thermal-Hysteresis	800nm	at low T: 6.60+1.83ι at middle T: 5.60+2.13ι 4.4+2.18ι at high T: 3.2+2.13ι
3. (ii)	50°C≤T≤80°C	Thermal-Hysteresis	1550nm	at low T: 8.10+1.60ι at middle T: -0.5+9.10ι 7.8+3.5ι at high T: -2.2+9.3ι

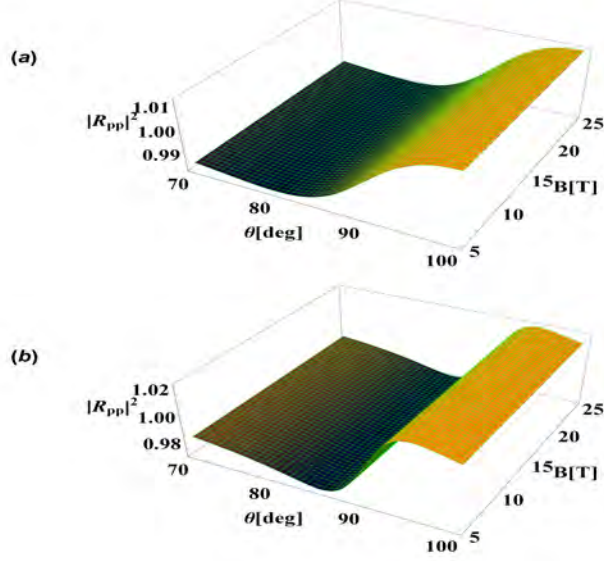Table 3.1: Brief Description of the Behavior of Temperature-Dependent Vanadium Dioxide.

Figure 3.1: Case 1(T $> 72°$C); The Effect of Incident Wavelength on Reflectance as a Function of Incident Angle, θ and Magnetic Field, B. At λ =800nm the Value of ϵ_b=-32.8+0.46ι in (a), at λ =1550nm the Value of ϵ_b=-140.4+3.56ι in (b), and the Value of Fermi Energy μ_F =450meV is Taken.

wavelength in a specific incident angle regime that agrees with the above statement in the previous figure.

Figure 4 is related to Case 2 and deals with the angular shifts by considering the same values of all parameters as in the previous one. In subfigure 4(a), the positive and negative angular shifts are observed at two different incident angles - one lying between 85 and 95 degrees and the other at a higher value beyond this range. Furthermore, in subfigure 4(b), when the incident wavelength increases, positive and negative GHS values around a higher angle are shifted towards that specific incident angle range. It is interesting to notice that modified angular GHS exhibits similar characteristics but with a greater amplitude as compared to Case 1. The difference between angular and modified angular shifts is sensitive to temperature and incident wavelength. This sensitivity cannot be ignored, as it provides significant positive and negative values that can be modulated both in and beyond the specific incident angle

11

ranges.

The angular shift is not only influenced by temperature and incident wavelength, it is also related to incident beamwidth. In Figure 5, the impact of beamwidth on angular shifts is examined for both cases 1 and 2, only for one wavelength value λ =800nm. The beamwidth is taken in micrometers produces shifts in kilo radians which is too large as compared to the above two figures where beamwidth is in millimeters. For angular GHS in both cases, positive and negative peaks approximately with the same widths are noticed which become narrow and disappear as the incident beamwidth increases. If modified angular GHS is analyzed only a negative peak is observed for Case 1 meanwhile, a positive peak with a narrow width and a negative peak with a widened width is noticed for Case 2. The positive peak becomes narrow whereas the negative peak becomes wider when the incident
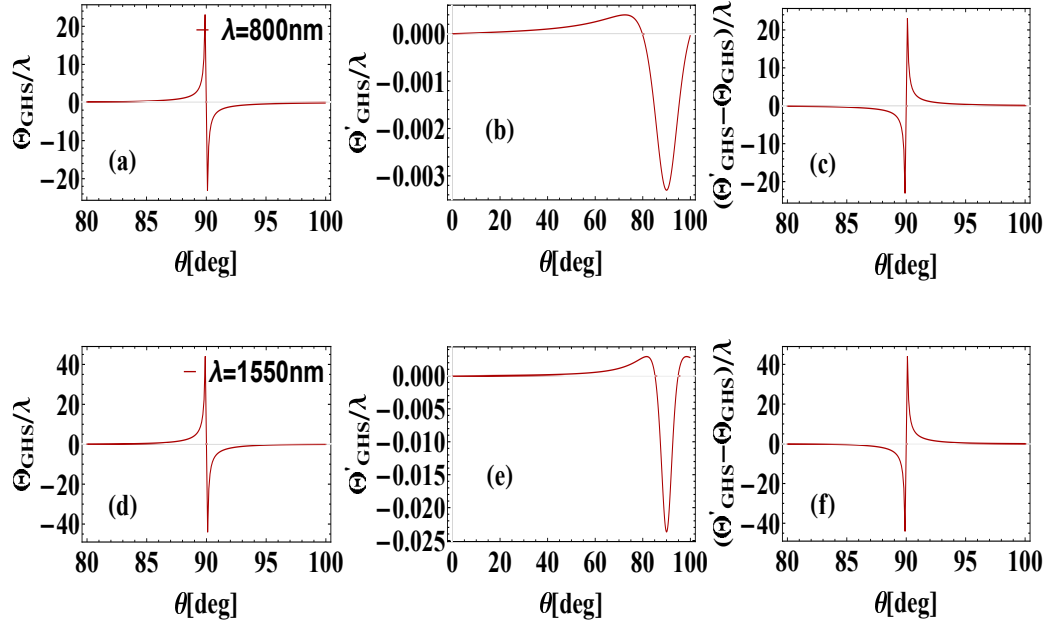
Figure 3.2: Case 1(T > 72°C); The Role of Incident Wavelength in Angular GHS, Θ_{GHS} (a), (d), Modified Angular GHS, Θ'_{GHS} (b), (e), and Their Difference, Θ'_{GHS}-Θ_{GHS}, (c), (f) as Function of Incident Angle in Degrees. The Value of ϵ_b=-32.8+0.46ι at λ =800nm in (a)-(c), Meanwhile at λ =1550nm the Value of ϵ_b=-140.4+3.56ι in (d)-(f), and the Value of Magnetic Field B =15T, Fermi Energy μ_F =450meV, and Beamwidth w =1mm is Taken.

Figure 3.3: Case 2(T < 58°C)); The Role of Incident Wavelength in Angular GHS, Θ_{GHS} (a), (d), Modified Angular GHS, Θ'_{GHS} (b), (e), and their Difference, Θ'_{GHS}-Θ_{GHS}, (c), (f) as Function of Incident Angle in Degrees. The Value of ϵ_b=32.8+0.46ι at λ =800nm in (a)-(c), Meanwhile at λ =1550nm the value of ϵ_b=140.4+3.56ι in (d)-(f), and the Value of Magnetic Field B =15T, Fermi energy μ_F =450meV, and Beamwidth w =1mm is Taken.
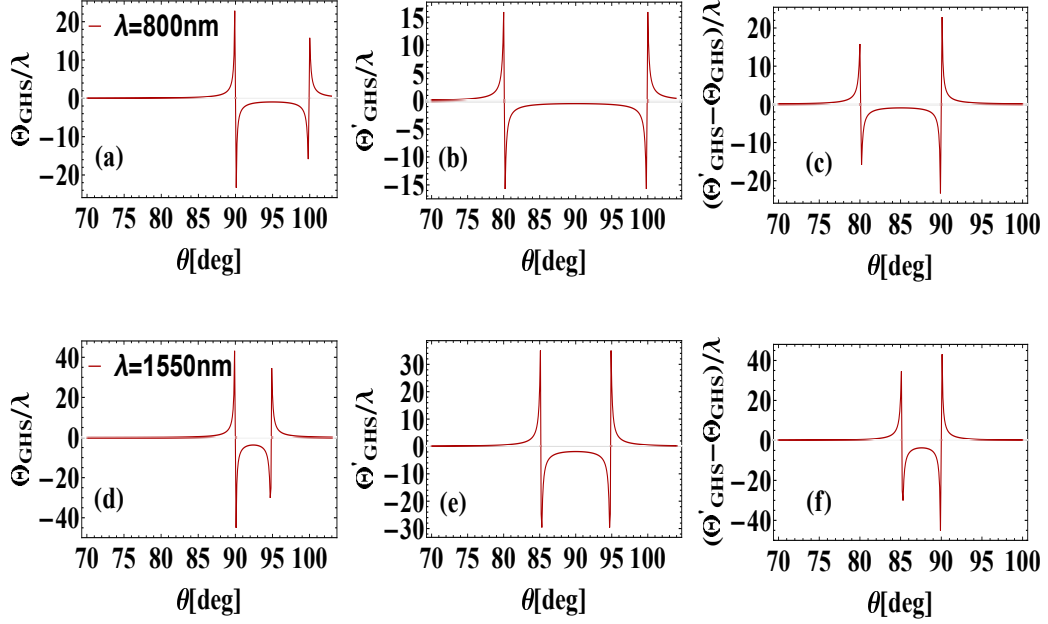
beamwidth increases. The narrow and widened width of angular shifts characterize strong and less sensitivity respectively, since it can be concluded that the incident beamwidth is very helpful in modulating angular shift according to application requirements.

The quantized Hall conductivity related to the graphene sheet strongly modulates the angular shift. The Landau levels are proportional to Fermi energy squared, but they are inversely proportional to the magnetic field plays a key role in the Hall conductivity and also affects GHS. From Figure 6, it can be seen that the Plataulike angular GHS increases as the Fermi energy decreases or the magnetic field increases. In subfigures 6(a) and (b), the difference of angular deviation is examined for incidence angle near and far away from the pseudo-Brewster angle respectively. Remarkably, the angular GHS for the incident angle near the pseudo-Brewster angle is greater at the
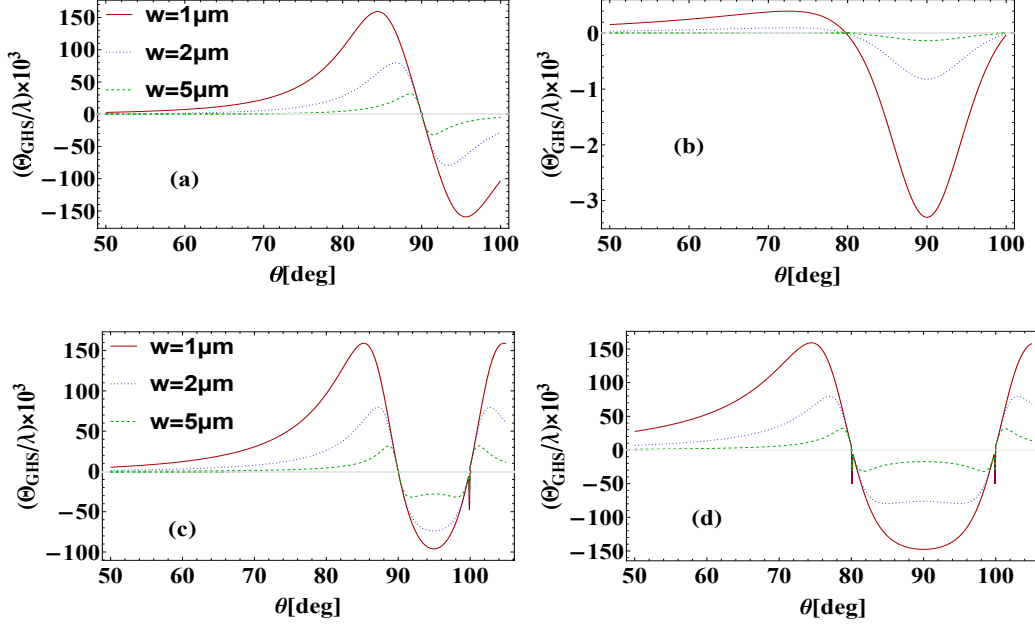
Figure 3.4: The Role of Incident Beamwidth and Wavelength in Angular GHS, Θ_{GHS} (a), (c), and Modified Angular GHS, Θ'_{GHS} (b), (d) as Function of Incident Angle in Degrees. The Red Solid Line, Blue Dotted Line, and Green Dashed Line Correspond to Incident Beamwidth $w = 1\mu m$, $2\mu m$, and $5\mu m$ Respectively. At $\lambda = 800$nm the Value of $\epsilon_b = -32.8 + 0.46\iota$ Case 1(T > 72°C) in (a), (b), Meanwhile, $\epsilon_b = 32.8 + 0.46\iota$ Case 2(T < 58°C) in (c), (d), and the Value of Magnetic Field $B = 15$T, and Fermi Energy $\mu_F = 450$meV is Taken.

same Fermi energy and magnetic field.

Finally, Case 3 is also studied to reveal the influence of Fermi energy and incident wavelength on angular shifts against the external magnetic field. From Figure 7, the quantized steps can be seen at smaller values of the magnetic field that exhibit strong sensitivity to change in Fermi energy. Furthermore, it may be noticed the quantized steps become narrow with rapid change as the Fermi energy increases which also agrees with the characteristics of shifts in the previous figure. Furthermore, positive angular GHS and negatively modified angular shift are obtained which can also be modulated by changing the incident wavelength.

14
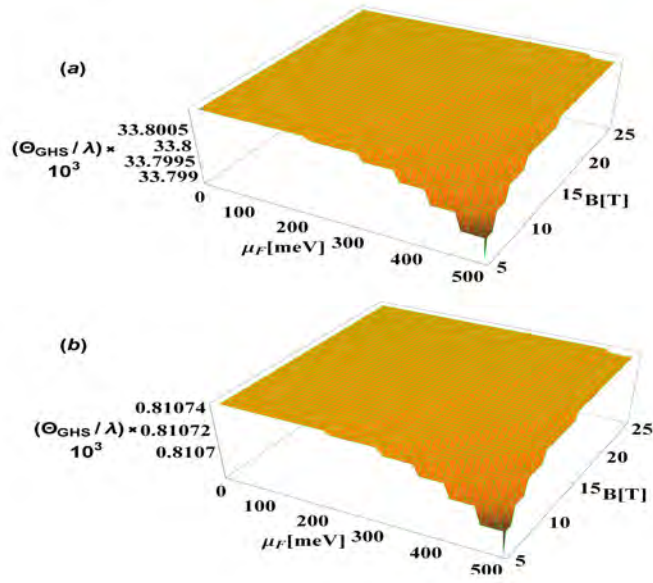
Figure 3.5: The Effect of Incident Angle $\theta = 71°$ in (a), Meanwhile, $\theta = 30°$ in (b) on Angular GHS, Θ_{GHS} as a Function of Fermi Energy, μ_F and Magnetic Field, B. At $\lambda = 800$nm the Value of $\epsilon_b = 32.8 + 0.46\iota$ Case 2(T $< 58°$C) and the Value of Beamwidth $w = 1\mu$m is Taken.
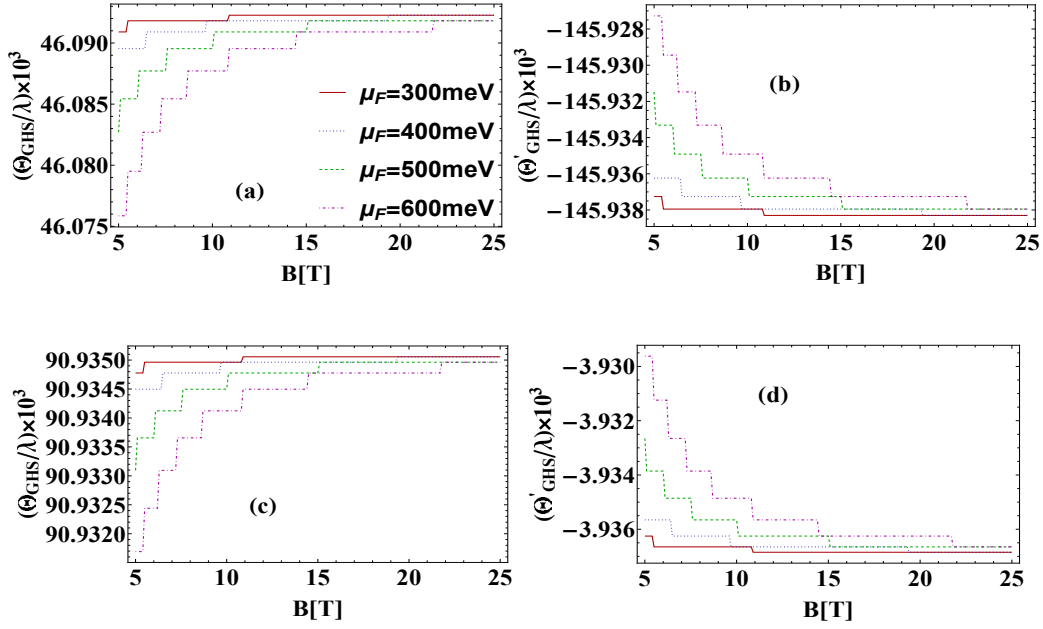
Figure 3.6: Case 3(50°C≤T≤80°C); The Role of Incident Wavelength and Fermi Energy in Angular GHS, Θ_{GHS} (a), (c), Modified Angular GHS, Θ'_{GHS} (b), (d) as Function of Magnetic Field. The Value of ϵ_b=6.6+1.83ι at λ =800nm in (a), (b), Meanwhile, at λ =1550nm the Value of ϵ_b=-0.5+9.1ι in (c), (d) and the Value of Incident Angle θ =71° (near Pseudo-Brewster Angle), and Beamwidth $w = 1\mu$m is Taken.

Chapter 4

Conclusion

The monochromatic Gaussian beam of light is excited on the graphene-vanadium dioxide interface, taking into account the temperature, wavelength, and dependency of graphene parameters, and reveals a quantized angular GH shift. For incident angles, the quantized steps of the angular GH effect have been greatly enhanced near the Brewster angle. The peaks of angular shifts become sharp as wavelength decreases. It has also been noted that incidence angle and beamwidth have an impact on the numbers mentioned previously, in addition to temperature and incident wavelength. It has been demonstrated that the cross-polarization component can not be ignored in the case of narrow quantized steps or for the incidence angle near the Brewster angle. Furthermore, by adjusting the Fermi energy and external magnetic field, the magneto-optical phenomena caused by Hall conductivity based on the graphene surface are also examined.

Bibliography

[1] Newton, I. (1952). Opticks, or, a treatise of the reflections, refractions, inflections & colours of light. Courier Corporation.

[2] Goos, F., & Hänchen, H. (1947). Ein neuer und fundamentaler Versuch zur Totalreflexion. Annalen der Physik, 436(7-8), 333-346.

[3] Artmann, K. (1948). Berechnung der Seitenversetzung des totalreflektierten Strahles. Annalen der Physik, 437(1-2), 87-102.

[4] Renard, R. H. (1964). Total reflection: a new evaluation of the Goos–Hänchen shift. JOSA, 54(10), 1190-1197.

[5] Yasumoto, K., & Oishi, Y. (1983). A new evaluation of the Goos–Hänchen shift and associated time delay. Journal of Applied Physics, 54(5), 2170-2176.

[6] Merano, M., Aiello, A., Van Exter, M. P., & Woerdman, J. P. (2009). Observing angular deviations in the specular reflection of a light beam. Nature Photonics, 3(6), 337-340.

[7] Emile, O., Galstyan, T., Le Floch, A., & Bretenaker, F. (1995). Measurement of the nonlinear Goos-Hänchen effect for Gaussian optical beams. Physical review letters, 75(8), 1511.

[8] Yin, X., & Hesselink, L. (2006). Goos-Hänchen shift surface plasmon resonance sensor. Applied physics letters, 89(26).

[9] Bretenaker, F., Le Floch, A., & Dutriaux, L. (1992). Direct measurement of the optical Goos-Hänchen effect in lasers. Physical review letters, 68(7), 931.

[10] Wang, L. G., Ikram, M., & Zubairy, M. S. (2008). Control of the Goos-Hänchen shift of a light beam via a coherent driving field. Physical Review A, 77(2), 023811.

[11] Ding, Y., Deng, D., Zhou, X., Zhen, W., Gao, M., & Zhang, Y. (2021). Barcode encryption based on negative and positive Goos-Hänchen shifts in a graphene-ITO/TiO2/ITO sandwich structure. Optics Express, 29(25), 41164-41175.

[12] Wang, J., Huang, H., Chen, C., He, H., Dong, Y., & Qi, H. (2013). Goos-Hänchen lateral displacements at the interface between isotropic and gyroelectric media. International Journal of Antennas and Propagation, 2013.

[13] Ziauddin, Chuang, Y. L., Qamar, S., & Lee, R. K. (2016). Goos-Hänchen shift of partially coherent light fields in epsilon-near-zero metamaterials. Scientific reports, 6(1), 26504.

[14] Wang, Y., Jamieson, S. M., & Perry, J. K. (2023). Targeting growth hormone in cancer: future perspectives. Endocrine-Related Cancer, 1(aop).

[15] Lakhtakia, A. (2004). Positive and negative Goos-Hauml; nchen shifts and negative phase-velocity mediums (alias left-handed materials). AEU-International Journal of Electronics and Communications, 58(3), 229-231.

[16] Waseer, W. I., Naqvi, Q. A., & Mughal, M. J. (2021). Goos-Hänchen shift at the planar interface of nid dielectric and topological insulator. Optik, 227, 166023.

[17] Ali, K., Syed, A. A., Waseer, W. I., & Naqvi, Q. A. (2021). Goos–Hanchen-effect for near-zero-index metamaterials excited by fractional dual fields. Optik, 243, 167501.

[18] Ali, N., Waseer, W. I., & Naqvi, Q. A. (2021). Analysis of Goos–Hanchen shift for an epsilon-near-zero slab sandwiched between two non-integer dimensional media. Optics Communications, 501, 127348.

[19] Manzoor, K. J., Naqvi, Q. A., & Mughal, M. J. (2022). Electrically tunable Goos–Hänchen shift from epsilon-near-zero (ENZ) structure with graphene. The European Physical Journal D, 76(12), 239.

[20] Ali, K., Waseer, W. I., & Naqvi, Q. A. (2022). Magnetic and fractional parametric control of Goos-Hänchen shifts in the anisotropic yttrium-iron-garnet film surrounded by isotropic fractal dielectric half-spaces. Physics Letters A, 453, 128496.

[21] Waseer, W. I., Naqvi, Q. A., & Mughal, M. J. (2020). Analysis of the Goos Hanchen shift for a planar interface of NID dielectric and general medium. Optik, 218, 165140.

[22] Nisar, M., Saghir, M. A., Shahzad, A., Waseer, W. I., & Naqvi, Q. A. (2022). Goos–Hanchen Shift in the presence of dispersive dielectric–magnetic medium using Lorentz–Drude Model. Optik, 262, 169273.

[23] Kravets, V. G., Grigorenko, A. N., Nair, R. R., Blake, P., Anissimova, S., Novoselov, K. S., & Geim, A. K. (2010). Spectroscopic ellipsometry of graphene and an exciton-shifted van Hove peak in absorption. Physical Review B, 81(15), 155413.

[24] Novoselov, K. S., Geim, A. K., Morozov, S. V., Jiang, D. E., Zhang, Y., Dubonos, S. V., ... & Firsov, A. A. (2004). Electric field effect in atomically thin carbon films. science, 306(5696), 666-669.

[25] Bocharov, A.A., 2022. Goos–Hänchen shift of a light beam tunable by graphene in the resonant optical tunneling structure. Journal of Optics, 24(11), p.115606.

[26] Wolf, E. L. (2014). Applications of graphene: an overview. Springer Science & Business Media.

[27] Neto, A. C., Guinea, F., Peres, N. M., Novoselov, K. S., & Geim, A. K. (2009). The electronic properties of graphene. Reviews of modern physics, 81(1), 109.

[28] Sarma, S. D., Adam, S., Hwang, E. H., & Rossi, E. (2011). Electronic transport in two-dimensional graphene. Reviews of modern physics, 83(2), 407.

[29] Ni, Z., Wang, Y., Yu, T., & Shen, Z. (2008). Raman spectroscopy and imaging of graphene. Nano Research, 1, 273-291.

[30] Taylor, P., Choi, W., Lahiri, I., & Seelaboyina, R. (2010). Synthesis of Graphene and Its Applications. Solid State Mater. Sci., 35(1), 52-71.

[31] Avouris, P. (2010). Graphene: electronic and photonic properties and devices. Nano letters, 10(11), 4285-4294.

[32] Giannazzo, F., Raineri, V., & Rimini, E. (2011). Transport properties of graphene with nanoscale lateral resolution. Scanning Probe Microscopy in Nanoscience and Nanotechnology 2, 247-285.

[33] Bonaccorso, F., Sun, Z., Hasan, T., & Ferrari, A. C. (2010). Graphene photonics and optoelectronics. Nature photonics, 4(9), 611-622.

[34] Zhan, B., Li, C., Yang, J., Jenkins, G., Huang, W., & Dong, X. (2014). Graphene field-effect transistor and its application for electronic sensing. Small, 10(20), 4042-4065.

[35] Liang, M., & Zhi, L. (2009). Graphene-based electrode materials for rechargeable lithium batteries. Journal of Materials Chemistry, 19(33), 5871-5878.

[36] Kang, X., Wang, J., Wu, H., Liu, J., Aksay, I. A., & Lin, Y. (2010). A graphene-based electrochemical sensor for sensitive detection of paracetamol. Talanta, 81(3), 754-759.

[37] Mohanty, N., & Berry, V. (2008). Graphene-based single-bacterium resolution biodevice and DNA transistor: interfacing graphene derivatives with nanoscale and microscale biocomponents. Nano letters, 8(12), 4469-4476.

[38] Li, T., Da, H., Du, X., He, J., & Yan, X. (2020). Giant enhancement of Goos–Hänchen shift in graphene-based dielectric grating. Journal of Physics D: Applied Physics, 53(11), 115108.

[39] Du, X., & Da, H. (2021). Large and controlled Goos–Hänchen shift in monolayer graphene covered multilayer photonic crystals grating. Optics Communications, 483, 126606.

[40] Song, Y., Wu, H. C., & Guo, Y. (2012). Giant Goos-Hänchen shift in graphene double-barrier structures. Applied Physics Letters, 100(25).

[41] Eick, H. A., & Kihlborg, L. A. R. S. (1966). The Crystal Structure of VOMo04. Acta Chem. Scand, 20(3), 9.

[42] Liu, M., Xie, S., Wei, L., Galluzzi, M., Li, Y., Wang, Q., ... & Li, J. (2020). Quantitative functional imaging of VO2 metal-insulator transition through intermediate M2 phase. Acta Materialia, 195, 720-727.

[43] Wall, S., Yang, S., Vidas, L., Chollet, M., Glownia, J. M., Kozina, M., ... & Trigo, M. (2018). Ultrafast disordering of vanadium dimers in photoexcited VO2. Science, 362(6414), 572-576.

[44] Lakhtakia, A., Wolfe, D. E., Horn, M. W., Mazurowski, J., Burger, A., & Banerjee, P. P. (2017, April). Bioinspired multicontrollable meta-surfaces and metamaterials for terahertz applications. In Bioinspiration, Biomimetics, and Bioreplication 2017 (Vol. 10162, pp. 140-145). SPIE.

[45] Waseer, W. I., & Lakhtakia, A. (2022). Thermal-hysteresis-affected surface-plasmon-polariton-wave propagation. Materials Letters, 324, 132648.

[46] Chao, D., Zhu, C., Xia, X., Liu, J., Zhang, X., Wang, J., ... & Fan, H. J. (2015). Graphene quantum dots coated VO2 arrays for highly durable electrodes for Li and Na ion batteries. Nano letters, 15(1), 565-573.

[47] Khan, Z., Singh, P., Ansari, S. A., Manippady, S. R., Jaiswal, A., & Saxena, M. (2021). VO2 nanostructures for batteries and supercapacitors: a review. Small, 17(4), 2006651.

[48] Liu, M., Su, B., Tang, Y., Jiang, X., & Yu, A. (2017). Recent advances in nanostructured vanadium oxides and composites for energy conversion. Advanced Energy Materials, 7Joushaghani49(23), 1700885.

[49] Joushaghani, A., Jeong, J., Paradis, S., Alain, D., Aitchison, J. S., & Poon, J. K. (2015). Wavelength-size hybrid Si-VO 2 waveguide electroabsorption optical switches and photodetectors. Optics express, 23(3), 3657-3668.

[50] Aiello, A., & Woerdman, J. P. (2008). Role of beam propagation in Goos–Hänchen and Imbert–Fedorov shifts. Optics letters, 33(13), 1437-1439.

[51] Luo, H., Ling, X., Zhou, X., Shu, W., Wen, S., & Fan, D. (2011). Enhancing or suppressing the spin Hall effect of light in layered nanostructures. Physical Review A, 84(3), 033801.

[52] Wu, W., Chen, S., Mi, C., Zhang, W., Luo, H., & Wen, S. (2017). Giant quantized Goos-Hänchen effect on the surface of graphene in the quantum Hall regime. Physical Review A, 96(4), 043814.